ISSN 0030-400X, Optics and Spectroscopy, 2015, Vol. 119, No. 1, pp. 146–154. © Pleiades Publishing, Ltd., 2015.
Original Russian Text © A.V. Pavlov, 2015, published in Optika i Spektroskopiya, 2015, Vol. 119, No. 1, pp. 151–159.

HOLOGRAPHY

The Influence of Hologram Recording Conditions and Nonlinearity of Recording Media on the Dynamic Characteristics of the Fourier Holography Scheme with Resonance Architecture

A. V. Pavlov

St. Petersburg State University of Information Technologies, Mechanics, and Optics, St. Petersburg, 197101 Russia
e-mail: pavlov@phoi.ifmo.ru

Received March 13, 2014; in final form, February 16, 2015

Abstract—A Fourier holography scheme in a ring cavity with two Fourier holograms (a matched hologram and a hologram in the correlation plane) has been considered. The dissipation factor of the scheme is determined, and the influence of the hologram recording conditions and the additional filtering caused by the nonlinearity of the exposure characteristics of holographic recording media on this parameter is demonstrated. It is also shown that high-frequency filtering on holograms reduces the convergence rate of the system to the stable state, whereas low-frequency filtering accelerates convergence. In the case of ultrahigh-frequency filtering or rejection of low frequencies, which destroys the internal correlatedness of images processed, the lateral maxima of the dissipation term grow. As result, under these filtering conditions, the dynamics of the system includes two successive stages: divergent (or pseudorandom) and convergent, in which the scheme converges to stable formation of image, which was absent during hologram recording. The results of numerical modeling for a number of models of hologram recording and additional filterings on holograms are presented.

DOI: 10.1134/S0030400X1507022X

INTRODUCTION

The Fourier holography scheme is widely used in optical information technologies. First of all, we should mention holographic correlators [1], which have gained a second wind in recent years due to the development of synthesized filters [2] for solving the problem of correlation algorithm sensitivity to geometric distortions and logic gates and processors [3], including devices implementing individual logical operations and fuzzy logics [4].

The classical 4*f* scheme (outlined by a dashed line in Fig. 1) is built based on a double Fourier transform cascade, formed by thin positive lenses L_1 and L_2. An interference pattern of the Fourier transforms of the images presented in the front focal plane of lens L_1 (input plane *In* of the scheme), standard image $Im_A(x, y)$ and reference image $Im_B(x, y)$, is formed in the rear focal plane of first Fourier transform lens L_1, which coincides with the front focal plane of lens L_2. Being recorded in an appropriate medium, this interference pattern forms a Fourier hologram. Let us assume the diffraction order of the hologram corresponding to the reference-beam propagation direction to be the +1st order. Then, as applied to the +1st diffraction order (the zeroth and –1st orders are disregarded), the Fourier hologram is described by the expression

$$H(\nu_x, \nu_y) = \eta(F(Im_B(x,y))\,F^*(Im_A(x,y))), \quad (1)$$

where (ν_x, ν_y) are spatial frequencies, η is an operator taking into account the nonlinearity of the exposure

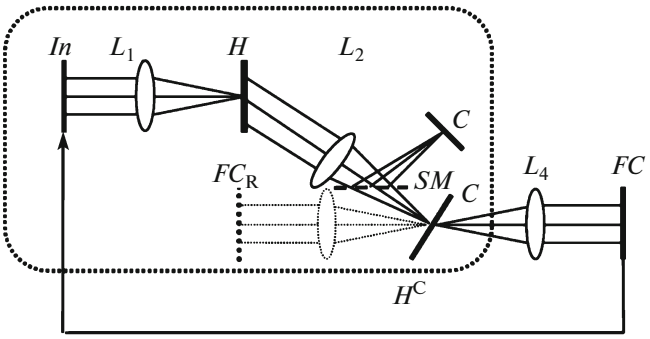

Fig. 1. 6*f* Fourier holography scheme with resonant architecture: (L_1, L_2, L_3, L_4) Fourier transform lenses; (H, H^C) matched hologram and hologram in the correlation plane, respectively; (*In*) input plane; (*C*) correlation plane; (*SM*) semitransparent mirror; and (FC_R) standard-image plane during recording hologram H^C; the cavity is closed with a video channel: $FC \rightarrow In$.

characteristics of holographic recording media, F is the Fourier transform symbol, and the asterisk denotes complex conjugation.

When an object image $Im_{Obj}(x, y)$ is formed in input plane In, the hologram response to the +1st diffraction order in the rear focal plane of second Fourier transform lens L_2 (correlation plane C) is described by the relation [1]

$$\begin{aligned} Im_C(\zeta,\eta) &= F\left[F\left(Im_{Obj}(x,y)\right)\right. \\ &\times \left.\eta\left(F\left(Im_B(x,y)\right)F^*\left(Im_A(x,y)\right)\right)\right] \\ &= \left[Im_{Obj}(x,y) \otimes Im_A(x,y)^* Im_B(x,y)\right]_\eta, \end{aligned} \quad (2)$$

where (ζ, η) are coordinates in correlation plane C (in contrast to the operator, the coordinates are given in italics); $\otimes$ and * are the symbols of correlation and convolution operations, respectively; and subscript η denotes additional filtering on hologram (1), which is caused by the nonlinearity of exposure characteristics of holographic recording media. If the reference image is a diffraction-limited point source ($Im_B(x, y) = \delta(x, y)$), the scheme is known as the Van der Lugt correlator [1]. If the reference image is not a point source ($Im_B(x, y) \neq \delta(x, y)$) and the object image is a point source ($Im_{Obj}(x, y) = \delta(x, y)$), i.e., hologram (1) is exposed to a plane wave front, the scheme is known as a joint transform correlator [2]. Both in the case of correlation image processing [1, 2] and when calculating logical reasoning [3, 4], field (2) is the summary response of the scheme: the result of processing according to these models is formed in one iteration: $In \rightarrow C$.

More complex models of data processing, e.g., models of autoassociative memory [5, 6], linear regression [7], plausible arguments (induction and abduction) [8], and nonmonotonic reasoning [9], can be implemented by making the scheme dynamic and, in some cases [8], removing the requirement for one from the three operands entering (2) to be a δ function. In view of the specificity of the journal *Optics and Spectroscopy*, we restrict ourselves to only optical aspects: analysis of the holographic scheme without detailed consideration of logic algebraic models. A reader interested in data processing models can find necessary information in the above-cited studies, including those specialized on artificial intelligence problems [8, 9].

To implement the dynamic mode, a 4*f* Fourier holography scheme is positioned in either a linear cavity, formed by phase-conjugate mirrors in the input and correlation [10] planes, or a ring cavity. The latter can be either purely optical or hybrid, including both a video channel [11] and a hologram in the C plane [9].

The best known application of the 4*f* Fourier holography scheme as a dynamic system is the implementation of the model of autoassociative memory in the phase-conjugation scheme [5, 6]. This application is based on the formal description of double Fourier transform cascade L_1, L_2 with hologram (1) by the model of external product of vectors $\mathbf{Im_A}$ and $\mathbf{Im_B}$, which are images in hologram recording, and further definition of the energy of the system as a particular case of a Lyapunov function [12] by the model of scalar product of vectors $\mathbf{Im_A}$ and $\mathbf{Im_{Obj}}$ (amplitude of the global maximum of autocorrelation function (ACF GM)), provided that hologram (1) is recorded with a flat reference beam; i.e., $Im_B(x, y) = \delta(x, y)$:

$$\mathscr{E} = -\left\langle \mathbf{Im_{Obj}} \mathbf{Im_A} \right\rangle = -\left(Im_{Obj}(x,y) \otimes Im_A(x,y)\right).$$

This model unambiguously determines the convergent character of dynamics [13], i.e., the stability of the response formed (reconstructed image); at the same time, it restricts the scheme application to only the memory concept: reconstruction of a standard pair of images $Im_A(x, y)$ and $Im_B(x, y) = \delta(x, y)$, in which hologram (1) was recorded. The implementation of more complex models of data processing [7–9] cannot be described within this formal approach.

Practical application of holographic information technologies calls for a tool allowing one to describe, as applied to the optical scheme, more complex (than only memory) processing models [7–9] and, in particular, determine the dynamics of a holographic scheme and its dependence on the characteristics of recorded holograms, which are determined by both the properties of holographic recording media and the recording conditions. An approach to solution of this problem can be based on the results of [14], which demonstrated that the stability of the response of Fourier holography scheme is determined by the presence of dissipation factor: Fourier transform. The dissipation factor is immanent to the algebraic model describing the holographic scheme [4]. Specifically optical aspects—the influence of the hologram recording conditions and properties of holographic recording media on the dynamics of the system—were not investigated in detail in [14].

In this study, which is a continuation of [4, 14], we consider the 4*f* Fourier holography scheme in a ring cavity, formed by a hologram in the correlation plane and a video channel (Fig. 1), as a generalized 6*f* scheme. Based on the introduction and analysis of the Lyapunov function of the system, we show that its dynamics depends on the characteristics of holographic recording media and the hologram recording conditions in the Fourier and correlation planes, including the properties of standard images for hologram recording.

OPTICAL SCHEME AND DYNAMICS

Let us present the classical 4*f* Fourier holography scheme in a linear cavity formed by phase-conjugate mirrors in the input (In) and correlation (C) planes as

a 6*f* scheme with hologram H^C recorded in the correlation plane:

$$H^C(\zeta,\eta) = \eta^C(F(Im_{FCR}(\chi_x,\chi_y))\, Im^*_{CR}(\zeta,\eta)), \quad (3)$$

where η^C is an operator taking into account the nonlinearity of the exposure characteristics of holographic recording media for hologram H^C; $Im_{FCR}(\chi_x,\chi_y)$ is the image in the FC_R, plane, which is used to record hologram H^C; $Im^*_{CR}(\zeta,\eta)$ is field (2), formed by the 4*f* scheme in the *C* plane; and subscripts *R* denote standard fields used to record hologram (3).

Here, we consider hologram H^C as a Fourier hologram recorded using a Fourier transform cascade with lens L_3 (shown by a dotted line in Fig. 1). This representation makes it possible to generalize the analysis to both linear and ring cavities, including implementation of more complex (than autoassociative memory [5, 6]) models [7–9, 13]. Specifically,

(i) if $Im_{FCR}(\chi_x,\chi_y) = \delta(\chi_x,\chi_y)$, we have a classical linear cavity, which is used to implement autoassociative memory [5, 6] and linear regression [7] models under exposure of hologram (3) to a wavefront that is complex-conjugate to the reference beam $F(Im_{FCR}(\chi_x,\chi_y))$;

(ii) for a ring cavity with an electron (video) channel [11] $C \to In$, term $Im_{FCR}(\chi_x,\chi_y)$ describes the pulsed response of the channel containing a hologram and closing the ring cavity; and

(iii) if $Im_{FCR}(\chi_x,\chi_y)$ is an image rather than a point source, we deal with the most general case, which covers, in particular, the nonmonotonic reasoning model [9, 14].

Let us consider the latter version. When an object image $Im_{Obj}(x, y)$ is present in input plane *In*, complex-amplitude field (2) is formed in the correlation plane; this field, being diffracted from hologram (3), forms the following field in the rear focal plane of lens L_4 (denoted below as the FC plane):

$$Im_{FC}(\chi_x,\chi_y) = F\{Im_C(\xi,\eta)\,\eta^C[F(Im_{FCR}(\chi_x,\chi_y))\, Im^*_{CR}(\zeta,\eta)]\}. \quad (4)$$

Field (4) is supplied to input plane *In* via an optical or video channel [11], and, as a result of the second iteration $In \to C$, a new amplitude field is formed in the *C* plane:

$$Im_{C2}(\zeta\eta) = Im_{FC}(\chi_x,\chi_y) \otimes Im_{A\eta}(x,y). \quad (5)$$

Let us impose the requirement of identity of the phase spectrum $\psi_{Obj}(\nu_x,\nu_y)$ of any object image to the phase spectrum of the standard on the set of object images $\{Im_{Obj}(x,y)\}$:

$$\forall Im_{Obj}(x,y) : \psi_{Obj}(\nu_x,\nu_y) = \psi_A(\nu_x,\nu_y). \quad (6)$$

This requirement is related to the specific algebraic model [15], the discussion of which is beyond the scope of our consideration.

Then, restricting ourselves to the ACF GM region, on the assumption of sufficient informativeness of processed images, which is estimated by the generalized spatial frequency $\Omega = S_A/S_{rA}$, where S_A is the standard area and S_{rA} is the standard correlation area [16, 17], we can neglect the noncommutativity property of the correlation. We assume also that

$$Im_{FCR}(\chi_x,\chi_y) \in \{Im_{Obj}(x,y)\}. \quad (7)$$

Conditions (6) and (7) provide unimodality (the presence of a pronounced GM) of field (5) and make it possible to simplify significantly (without loss of generality) further expressions by replacing the (χ_x,χ_y) coordinates in the FC_R plane with the (x,y) coordinates. Then, expression (5) takes the following form for the *n*th iteration (we omit simple but cumbersome intermediate transformations):

$$Im_{Cn}(\zeta,\eta) = F\left(Im_{Cn-1}(\zeta,\eta)\right)^* \times \left\{\left[Im_{FCR\eta^C}(x,y) \otimes F(Im_{CR}(\zeta,\eta))\right] \otimes Im_{A\eta}(x,y)\right\}. \quad (8)$$

Using conditions (6) and (7), we introduce ordering relationship $\overset{\alpha}{\prec}$ on the set of processed images $\{Im_{Obj}(x,y)\}$ in the following way:

$$\forall Im_k(x,y), Im_l(x,y) \in \{Im_{Obj}(x,y)\} : Im_k(x,y) \overset{\alpha}{\prec} Im_l(x,y) \Leftrightarrow r_{k\alpha} < r_{l\alpha}, \quad (9)$$

where $r_{k\alpha}$, $r_{l\alpha}$ are the correlation lengths of the *k*th and *l*th images, respectively, measured at the level $\alpha;\alpha \in [\upsilon,1]$, $[\upsilon,1]$ is the interval of normalized ACF GM amplitudes, and υ is the maximum amplitude of ACF lateral maxima. The advantages of this way of introducing order are as follows:

(i) universality in the sense of applicability to a wide class of images and signals;

(ii) allowance for the internal correlatedness (as a property of information distinguishing it from noise) and its changes as a result of filtering;

(iii) possibility of determining ordering relationship (9) in the Fourier space

$$Im_k(x,y) \overset{\alpha}{\prec} Im_l(x,y) \Leftrightarrow r_{k\alpha} < r_{l\alpha} \Leftrightarrow |F(Im_k(x,y))|_\beta > |F(Im_l(x,y))|_\beta,$$

where $|F(Im_k(x,y))|_\beta$ is the radius of the amplitude spectrum at level $\beta;\beta \in [0,1]$.The weak points of this way of introducing order are determined by the fact that filtering is often accompanied by a change in the

shape of ACF GM [18] and, therefore, sign $\prec$ or $\succ$ may change, depending on the α value. We assume, furthermore, that this fact is taken into consideration and apply ordering relationship (9) to all complex-amplitude fields under analysis.

Let us determine the Lyapunov function [12] for the 6*f* scheme. We have the classical version for the $In \to C$ iteration: the double Fourier transform cascade L_1, L_2 with hologram (1) is described by the model of external product of vectors $\mathbf{Im_A}$ and $\mathbf{Im_B}$. Due to this, one can introduce [13] energy for this iteration according to the model of the scalar product of vectors $\mathbf{Im_{In}}$ and $\mathbf{Im_C}$, which describe the current distribution of amplitudes in the corresponding planes [19]:

$$\mathcal{E}_{InC} = -\langle \mathbf{Im_{In}} \mathbf{H} \mathbf{Im_C} \rangle \propto = -(Im_{In}(x,y) \otimes Im_{A\eta}(x,y)^* Im_{B\eta}(x,y) \otimes Im_C^*(x,y)). \quad (10)$$

In (10) and below, the field in the *In* plane is denoted using subscript *In* rather than *Obj*, which was used previously, because the latter is applicable to only the first iteration.

For the $C \to In$ iteration, the direct introduction of the energy function in a similar way (as a particular case of the Lyapunov function) is incorrect, because, in this case, the *C* and *In* planes are related by only a single Fourier transform. However, we can consider the double Fourier transform cascade L_2, L_4 with hologram (3). This cascade implements the model of external product of vectors $\mathbf{F}(\mathbf{Im_C})$ and $\mathbf{Im_{In}}$; correspondingly, one can introduce the Lyapunov function for this cascade and the $H \to In$ iteration in a similar way (for brevity, we omit below designations of coordinates):

$$\mathcal{E}_{HIn} = -\langle \mathbf{F}(\mathbf{Im_C}) \mathbf{H}^C \mathbf{Im_{In}} \rangle \propto -(F(Im_{In})\eta(F^*(Im_A)) \times [F(\eta^C)^*(F^*(Im_{InR})\eta(F(Im_A)))^* Im_{FCR}] Im_C^*), \quad (11)$$

where Im_{InR} is the image used in the *In* layer to form field Im_{CR} by hologram (1) when recording hologram (3).

Component $\mathcal{E}_{InC}$ determines the convergence of the dynamics of the scheme in Fig. 1 [12] as the convergence to the stable state corresponding to the fields in the *In* and *C* planes:

$$\begin{cases} Im_{In}(x,y) \to Im_A(x,y) \otimes Im_B(x,y) \\ Im_C(\zeta,\eta) \to \delta(\zeta,\eta). \end{cases} \quad (12)$$

If hologram (1) is recorded with a flat reference beam, $Im_B(x,y) = \delta(x,y)$, the stable state of the system corresponds to the reconstruction of the standard:

$$Im_{In}(x,y) \to Im_A(x,y).$$

The *H* and *C* planes are related by the Fourier transform; therefore, component $\mathcal{E}_{HIn}$ determines the dynamics of the scheme as the convergence to the state

$$\begin{cases} F(Im_C(\zeta,\eta)) \to F\left(Im_{CR}(\zeta,\eta)\right), \\ Im_{In}(x,y) \to Im_{InR}(x,y). \end{cases} \quad (13)$$

Thus, components $\mathcal{E}_{InC}$ and $\mathcal{E}_{HIn}$ determine opposite directions of the dynamics of the system in the $In \to C$ (12) and $C \to In$ (13) iterations.

INFLUENCE OF HOLOGRAM RECORDING CONDITIONS ON THE DYNAMICS OF THE SCHEME

To analyze the factors affecting the dynamics of the system (which are determined by the hologram recording conditions and the properties of holographic recording media), we return to expression (8). The relationship of the field in the *n*th iteration (8) with the result of the previous ($(n-1)$th) iteration through the Fourier transform determines the dynamics cyclicity. If

$$Im_{Cn}(\zeta,\eta) \overset{\alpha}{\succ} F\left(Im_{C(n-1)}(\zeta,\eta)\right),$$

in the *n*th iteration,

$$Im_{C(n+1)}(\zeta,\eta) \overset{\alpha}{\prec} F\left(Im_{Cn}(\zeta,\eta)\right),$$

in the $(n+1)$th iteration and vice versa. The expression in braces in (8),

$$\left\{\left[Im_{FCR\eta^C}(x,y) \otimes F(Im_{CR}(\zeta,\eta))\right] \otimes Im_{A\eta}(x,y)\right\}, \quad (14)$$

is independent of the iteration number and plays the role of dissipation term, which is responsible for the oscillation damping (12) $\leftrightarrow$ (13) as convergence to the stable state. At the minimum value of the dissipation term,

$$\left\{\left[Im_{FCR\eta^C}(x,y) \otimes F(Im_{CR}(\zeta,\eta))\right] \otimes Im_{A\eta}(x,y)\right\} = \delta,$$

the system would have a stable cyclic dynamics; an increase in the value of (14) should lead to an increase in the oscillation damping rate. Let us now analyze the role of the operands entering (14) and their contribution to the dynamics.

The first operand $Im_{FCR\eta^C}(x,y)$ describes the conditions for recording hologram (3), which include the choice of standard image $Im_{FCR}(x,y)$ and the hologram recording and processing conditions providing additional filtering [18]. It obviously follows from (14) that $Im_{FCR\eta^C}(x,y)$ and dissipation term (14) as a whole are isotonic.

The influence of the choice of standard $Im_{FCR}(x,y)$ on the dissipation term is determined by

the fact that, according to (12) and with allowance for the introduced ordering relationship (9),

$$i < j \Leftrightarrow Im_{FCi}(x,y) \overset{\alpha}{\prec} Im_{FCj}(x,y).$$

Correspondingly, if

$$Im_{FCR}(x,y) = \min\{Im_{FC}(x,y)\}; \quad (15)$$

i.e., according to (9), standard $Im_{FCR}(x,y)$ is the highest frequency one from set $\{Im_{FC}(x,y)\}$, and dissipation term (14) is minimized on the whole and vice versa.

The recording and processing conditions for hologram (3) determine additional filtering, which is caused by the nonlinearity of exposure characteristics of holographic recording media [18]. According to (12), high-frequency filtering has as a consequence

$$Im_{FCR\eta^c}(x,y) \overset{\alpha}{\prec} Im_{FCR}(x,y)$$

and a decrease in dissipation term (14). In contrast, low-frequency filtering leads to

$$Im_{FCR\eta^c}(x,y) \overset{\alpha}{\succ} Im_{FCR}(x,y);$$

an increase in dissipation term (14); and, correspondingly, an increase in the convergence rate.

The second operand describes the response of hologram (1) directly behind its plane in the stage of recording hologram (3):

$$F(Im_{CR}(\zeta,\eta)) = F(Im_{InR}(x,y))H(\nu_x,\nu_y) = F(Im_{InR}(x,y))\eta(F(Im_B(x,y))F^*(Im_A(x,y))). \quad (16)$$

It follows from (16) that the second operand takes into account the following:

(i) the conditions for recording hologram (1), concerning the choice of standards $Im_A(x,y)$ and $Im_B(x,y)$;

(ii) the conditions for recording hologram (1), concerning the choice of its recording and processing conditions, which determine the additional filtering, described by operator η; and

(iii) the conditions for reconstructing hologram (1), concerning the choice of object image $Im_{InR}(x,y)$ to form its response, which is used during recording of hologram (3), and, correspondingly, the conditions for recording hologram (3).

Since fields $Im_A(x,y)$, $Im_B(x,y)$, and $Im_{InR}(x,y)$ enter (16) via their Fourier transforms, in view of (12), they are antitonic to the second operand. The second operand, in turn, has an algebraic sense of subtracted [4] and, therefore, is antitonic to term (14) as a whole. Correspondingly, high-frequency filtering on hologram (1) leads to an increase in the second operand and a decrease in the convergence rate of the system; on the contrary, low-frequency filtering increases the convergence rate. Note that the antitonicity of the second operand to dissipation term (14) can be violated with an increase in the filtering frequency on holograms (1) and (3) (rejection of low frequencies) due to the violation of unimodality (which follows from (7)) of dissipation term (14) and response (8) of the scheme due to the increase in the ACF lateral maxima above the ACF GM level.

The expression in square brackets describes the pulsed response of hologram (3) and depends on both its recording conditions (including the choice of standard $Im_{FCR}(x,y)$) and on the conditions of recording hologram (3) (the second term).

The third operand depends on only the conditions of recording hologram (1); it is isotonic to both the first operand and term (14) as a whole. High-frequency filtering on hologram (1) may also lead to an increase in the lateral maxima of its response (8), up to loss of unimodality with growth of ACF lateral maxima.

NUMERICAL MODELING

We modeled the operation of the 6*f* scheme (Fig. 1) during recording of hologram (3) according to condition (7). The influence of the recording conditions, concerning the choice of the coincidence rate of local beam amplitudes [16–18], was modeled by introducing an additional Gaussian (high- or low-frequency) filter, with limitation of the hologram dynamic range to two orders of magnitude in the case of high-frequency filtering. Three types of holograms (3) were modeled:

(i) a linear hologram (with additional filtering);

(ii) a hologram with the spectrum of the image (described by the first operand) presented as white; i.e., with the amplitude spectrum of constant density:

$$\left|F\left(\mathrm{Im}_{FCR\eta^c}(x,y)\right)\right| = \mathrm{Const}(\zeta,\eta), \quad (17)$$

and

(iii) a hologram with white spectra for both beams; i.e., in addition to (17), the following condition is fulfilled:

$$C_R(\zeta,\eta) = \mathrm{Const}(\zeta,\eta). \quad (18)$$

Images were modeled by realizations of random processes (2048 counts long), with amplitude spectra described by Gaussian functions, and random phase spectra with normal distribution in the interval $[0, 2\pi]$. The characteristics of additional filtering on holograms (1) and (3) and the corresponding ACF GM lengths for standard realization $Im_A(x)$ are given in Table 1.

To evaluate the scheme with allowance for additional filterings, dissipation factor (14), and individual operands, we used, according to the introduced ordering relationship (9), their correlation lengths. The

Table 1. Characteristics of additional Gaussian filters and standard images for modeling the nonlinearity of holograms (1) and (3)

No.	$Im_A\, r_{0.606}$ (pixels)		Additional-filter parameters		
	(a)	(b)	Type	ν_0	$\nu_{0.606}$
1	12	8	HF	30	20
2	13	9	HF	20	20
3	13	9	HF	10	20
4	14	9	No	–	–
5	14	10	LF	40	40
6	19	17	LF	30	40
7	24	19	LF	20	40
8	29	28	LF	20	20

dynamics was estimated by calculating (i) extinction coefficient γ, which is given by the expression [20]

$$|r_{0.606}(n) - r_{0.606}(n-1)| = y_0 + \exp(\gamma n), \qquad (19)$$

where r are the lengths of the global maxima of the response (field (8)) at a level of 0.606 in corresponding iterations and n is the iteration number, and (ii) logarithmic decrement [20]

$$\delta_l = \ln \frac{|r_{n-1} - r_n|}{|r_{n+1} - r_n|}.$$

Figure 2 shows the dependences of the extinction coefficient (19) on the length of the ACF GM for dissipation term (14), determined by filtering on holograms (1) and (3), for the three aforementioned models of hologram (3). In the region of monotonic dependence of the extinction coefficient on the length of the ACF GM for the dissipation term, calculation

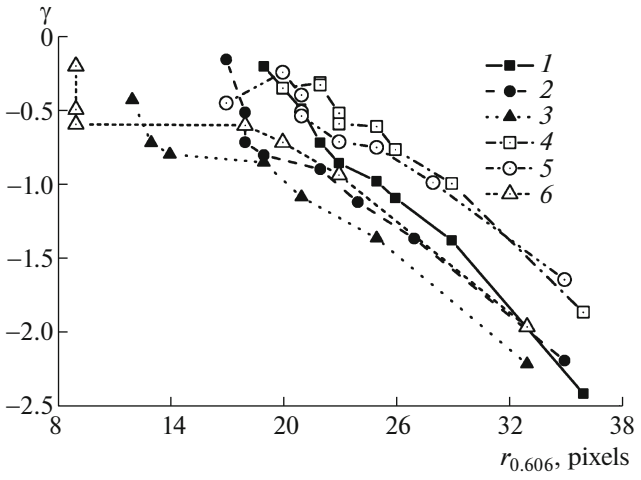

Fig. 2. Dependences of the extinction coefficient on the ACF GM length for dissipation term (14), under conditions of Table 1.

points were approximated by a linear dependence; the slopes for series (a) turned out to be 0.115 (linear hologram (3)), 0.103 (17), and 0.104 (18); i.e., the slopes can be considered approximately equal accurate to the second decimal place.

In the region of high-frequency filtering, the monotonic dependence of the extinction coefficient on the ACF GM length for the dissipation term is violated. The reason is that pronounced lateral maxima (even with amplitudes exceeding the global maximum amplitude) arise in the dissipation term (14); correspondingly, the unimodality of response (8) of the scheme is violated. For illustration, Figs. 3a and 3b present cross sections of dissipation term (14) and its ACF at the filtering parameters given in row 1 of Table 1 (series a) and for filtering parameters $\nu_0 = 40$ and $\nu_{0.606} = 6$, which in fact correspond to rejection of low frequencies. One can clearly observe violation of unimodality of the dissipation term and its ACF: growth of lateral maxima at ultrahigh-frequency filtering on hologram (1). It can be seen in Figs. 3a and 3b that the region of high-frequency filtering is characterized by violation of both the monotonic dependence of the effective size of dissipation term (Fig. 3a) and the estimate of its value by the ACF GM length (Fig. 3b). This effect increases when passing from attenuation (curves *1–3*) to rejection (curves *4–6*) of low frequencies.

Figures 4a and 4c show the dynamics of the system for row 1 of Table 1, and Figs. 4b and 4d present the dynamics for the case of rejection of low frequencies on hologram (1). To make the plots less cumbersome, the dynamics for model (18) of hologram (3), which differs from the dynamics for the linear model and model (17), is shown separately in Figs. 4c and 4d. Figure 4a demonstrates classical convergent dynamics, whereas Fig. 4b illustrates the change in the dynamics type: from divergent in the initial stage to convergent in the second stage. The ACF GM length of the object image was 105 pixels; the pulsed response of the scheme amounted to 9 pixels; and the ACF GM lengths for the dissipation factor for models of holograms (3) were 11 pixels for the linear type, 10 pixels for type (17), and 9 pixels for type (18). Figure 5 presents dependences of the logarithmic decrement on the iteration number, which clearly illustrate the change in the dynamics type.

It can be seen in Fig. 4b that the GM length in the *C* plane, which exceeds the initial value, corresponds to the stable state. This fact is explained in Fig. 6: the reason is in violation of the unimodality of image (8) with an increase in the amplitude of lateral maxima, which are now recorded instead of the GM. Figure 6a shows images (8) (formed according to the main derivation rules) for four object images; the corresponding characteristics are listed in Table 2. Figure 6b presents responses for the model of linear hologram (3) in the zeroth, 2nd, 5th, 6th, 7th, 8th, 11th, and 30th iterations, which demonstrate increasing violation of uni-

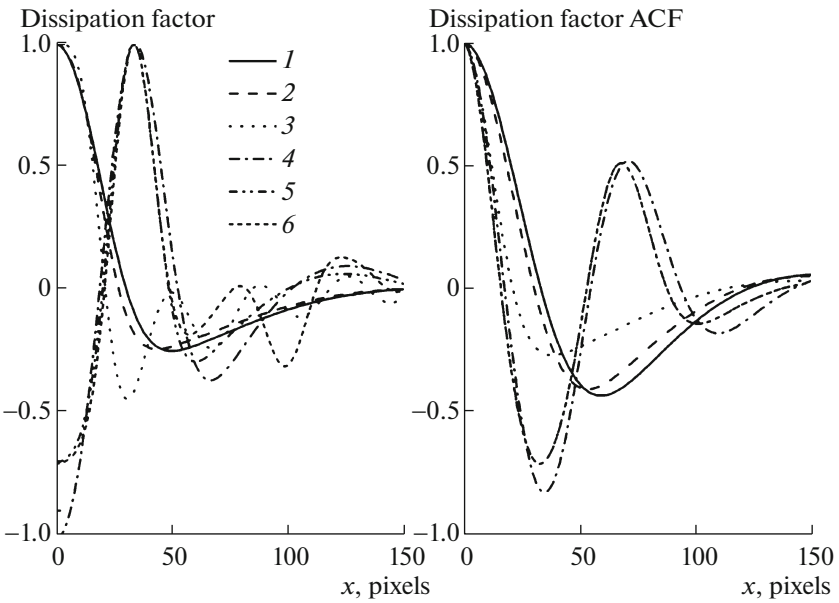

Fig. 3. (a) Cross sections of the dissipation factor for filterings on hologram (1), (*1–3*) row 1 of Table 1 and (*4–6*) $\nu_0 = 40$ and $\nu_{0.606} = 6$, and conditions for recording hologram (3): (*1*, *4*) linear type, (*2*, *5*) type (17), and (*3*, *6*) type (18). (b) Cross sections of the dissipation factor ACF under the same conditions as for panel a.

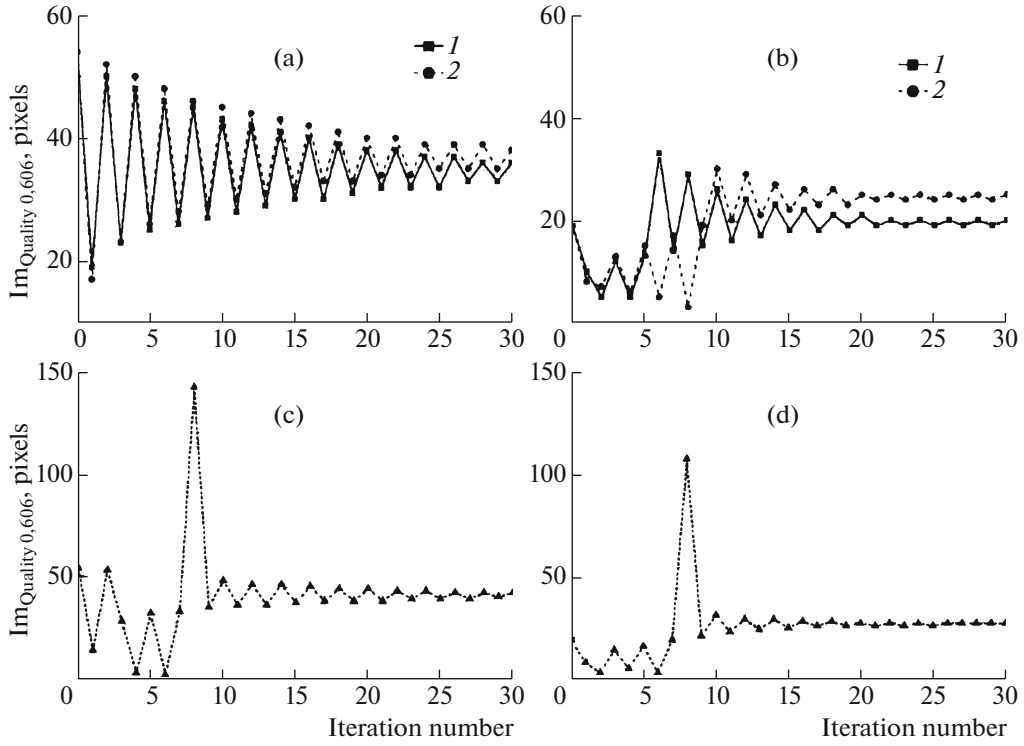

Fig. 4. Examples of optical scheme dynamics: dependences of the GM FWHM on the iteration number for different hologram recording conditions: (a) in the Fourier plane (hologram (1), row 1 of Table 1) and in the correlation plane (hologram (3): (*1*) linear type and (*2*) with spectrum turned white according to model (17)); (b) with rejection of low frequencies on the hologram in the Fourier plane; the hologram recording conditions and designation are the same as for panel a; (c) in the Fourier plane (hologram (1), row 1 of Table 1) and in the correlation plane (hologram with spectrum turned white according to model (18)); and (d) with rejection of low frequencies on the hologram in the Fourier plane (the hologram recording conditions are the same as for panel c).

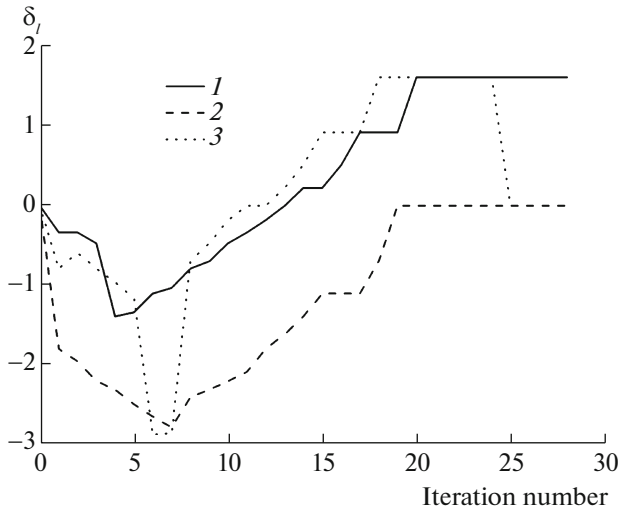

Fig. 5. Dependences of the logarithmic decrement on the iteration number for different types of holograms (3): (*1*) linear type, (*2*) type (17), and (*3*) type (18).

modality of image (8) with a subsequent step change in the type of dynamics and attainment of stable state at a new level; the image is stabilized with lateral maxima exceeding the global one. In the above-reported example, the ratio of the lateral maximum amplitude to the GM amplitude in the stable mode turned out to be 1.503.

A comparison of Table 2 and Fig. 6a shows that, in the case of rejection of low frequencies, the ACF GM length is not an adequate estimate of the information properties of the image arriving at hologram (3) for further processing, because it disregards the destruction of internal correlatedness, which manifests itself in the presence of lateral correlation function maxima, comparable with the ACF GM. In this case, the destruction of internal correlatedness during rejection of low frequencies is more pronounced for initially lower frequency images (Table 2).

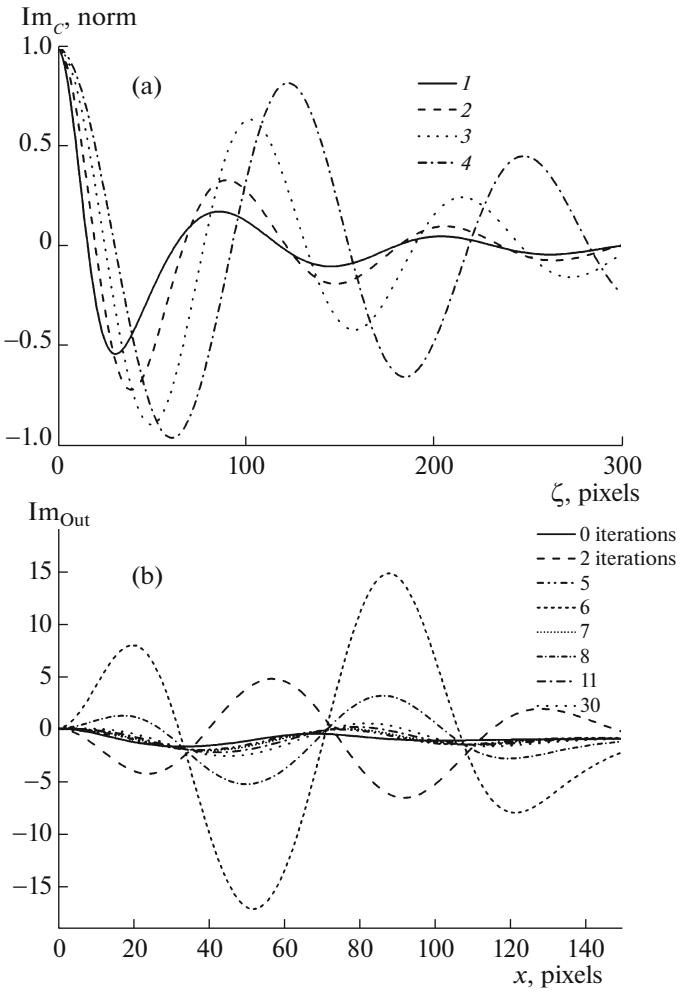

Fig. 6. (a) ACFs of the images filtered by hologram (1) according to Table 2 and (b) images (8), formed by the system in the zeroth, 2nd, 5th, 6th, 7th, 8th, 11th, and 30th iterations.

Table 2. Characteristics of object images and images filtered by hologram (1) in the case of rejection of low frequencies (Fig. 6)

Curve number	$r_{0.606}$ for object image	$r_{0.606}$ for hologram (1)
1	14	9
2	27	11
3	53	15
4	105	18

CONCLUSIONS

Thus, the Fourier holography scheme with resonant architecture can be modeled by the 6*f* scheme, which generalizes both linear and ring cavities, including ring cavities closed by a video channel. The fundamental physical phenomenon of diffraction is responsible for the dissipative character of the scheme and, correspondingly, the convergent type of dynamics. The convergence rate of the system to the stable state is affected by the characteristics of standard images for hologram recording and the properties of holographic recording media and hologram recording conditions. Low-frequency filtering increases the convergence rate, whereas high-frequency filtering, on the contrary, reduces it. In the case of ultrahigh-frequency filtering (determined according to the criterion of destruction of the internal correlatedness of images), the dynamics of the system becomes catastrophic: it is divergent in the first stage and then changes to convergent; however, the image formed in the stable state does not satisfy the requirement for unimodality, which is necessary for the logical reasoning pattern. In other words, in the case of ultrahigh-frequency filtering on a hologram, the application of the above-described scheme in logical data processing models is problematic. This conclusion is consistent with the results obtained previously by E.I. Shubnikov et al. [16–18], according to which ultrahigh-frequency filtering leads to a catastrophic decrease in the signal-to-interference ratio and transformation of information into noise.

ACKNOWLEDGMENTS

This study was supported by the Russian Foundation for Basic Research, projects nos. 12-01-00418-a and 15-01-04111-a.

REFERENCES

1. G. I. Vasilenko and L. M. Tsibul'kin, *Holographic Recognition Devices* (Radio i Svyaz', Moscow, 1985) [in Russian].
2. N. N. Evtikhiev, S. N. Starikov, D. V. Shaulskiy, R. S. Starikov, and E. Yu. Zlokazov, Opt. Eng. **50** (6), 065803 (2011).
3. E. Gur, D. Mendlovic, and Z. Zalevsky, Appl. Opt. **37** (29), 6937 (1998).
4. A. V. Pavlov, Opt. Spectrosc. **90** (3), 452 (2001).
5. E. G. Paek and D. Psaltis, Opt. Eng. **26**, 428 (1987).
6. Y. Owechko, G. J. Dunning, E. Marom, and B. H. Soffer, Appl. Opt. **26**, 1900 (1987).
7. A. V. Pavlov, Opt. Spectrosc. **98** (6), 949 (2005).
8. A. V. Pavlov, Iskusstv. Intellekt Prinyatie Reshenii, No. 1, 3 (2010).
9. A. V. Pavlov, Iskusstv. Intellekt Prinyatie Reshenii, No. **3**, 26 (2012).
10. V. Yu. Venediktov, G. E. Nevskaya, and M. G. Tomilin, Opt. Spectrosc. **111** (1), 113 (2011).
11. A. A. Leshchev, V. A. Berenberg, M. V. Vasil'ev, V. Yu. Venediktov, N. L. Ivanova, Yu. A. Petrushin, P. Semenov, and N. N. Freigang, Kvantovaya Elektron. **37** (8), 716 (2007).
12. G. A. Korn and T. M. Korn, *Mathematical Handbook for Scientists and Engineers* (McGraw-Hill, New York, 1968).
13. N. A. Magnitskii, Dokl. Akad. Nauk **338** (3), 320 (1994).
14. A. V. Pavlov, Nauch. Tekh. Vestn. Inf. Tekhnol., Mekh., Opt., No. 1 (89), 17 (2014).
15. A. V. Pavlov, *Proc. V Int. Sci.–Practical Conf. "Integrated Models and Soft Calculations in Artificial Intelligence," 28–30 May, 2009,* Vol. 1, p. 140.
16. E. I. Shubnikov, Opt. Spektrosk. **62** (2), 450 (1987).
17. E. I. Shubnikov, Opt. Spektrosk. **62** (3), 653 (1987).
18. A. M. Kuleshov and E. I. Shubnikov, Opt. Spektrosk. **60** (3), 606 (1986).
19. B. Kosko, Appl. Opt. **26**, 4947 (1987).
20. V. V. Dubnishchev, *Vibrations and Waves* (Lan', St. Petersburg, 2011) [in Russian].

Translated by Yu. Sin'kov